Available online at www.sciencedirect.com
ScienceDirect
Journal of the European Ceramic Society 31 (2011) 1177–1185
www.elsevier.com/locate/jeurceramsoc

Original Article

Microbial corrosion of silicon nitride ceramics by sulphuric acid producing bacteria *Acidithiobacillus ferrooxidans*

Detlef Dierksen *, Petra Kühner, Andreas Kappler, Klaus G. Nickel

Eberhard Karls Universität Tübingen, Institute for Geoscience, Sigwartstrasse 10, 72076 Tübingen, Germany

Received 24 June 2010; received in revised form 26 November 2010; accepted 1 December 2010
Available online 13 January 2011

Abstract

Yttria/alumina doped silicon nitride ceramics were exposed to corrosive *Acidithiobacillus ferrooxidans* bacteria cultures. These microorganisms produce sulphuric acid as a metabolic product during thiosulfate oxidation. In this study, the effect of microbial corrosion of silicon nitride ceramics is compared with an abiotic-chemical corrosion process in sulphuric acid under similar conditions (e.g. pH, temperature and exposure time). While abiotic corrosion caused only partial lixiviation of the superficial grain boundary phase, microbially induced corrosion lead to an almost total dissolution of the amorphous grain boundary within the corrosion zone. Microbial corrosion is thus more efficient than the abiotic process: it dissolves more silica and causes therefore a higher corrosion rate. This is probably due to the additional microbial release of metal-chelating organic compounds that stimulate the corrosion process.

Keywords: Silicon nitride; Bacteria; Microbial corrosion; Sulphuric acid; Corrosion kinetics

1. Introduction

Silicon nitride ceramics (Si_3N_4) are well known to show high corrosion stability as well as enhanced temperature and oxidation resistances under extreme conditions. Sintered Si_3N_4-ceramics typically consist of ≥90 weight percent of β-Si_3N_4-grains and an amorphous grain boundary phase (GBP). This GBP is composed of silica and/or oxynitride and contains additional metal oxides (e.g. Al_2O_3, Y_2O_3 and MgO), typically added as sintering additives.[1] The GBP can be divided into two distinct parts, (1) the stable film at the grain boundaries which reaches a thickness between 0.5 and 2 nm between individual grains in direct contact[1,2] and, (2) the glass pockets in triple points between several grains. These two parts of the GBP usually differ from each other e.g. in terms of their chemical composition.[1]

Silicon nitride ceramics are often used under high temperature conditions in engines but also in chemical plants, where the material is exposed to extreme chemicals including strong inorganic acids and bases. Concerning the latter applications, numerous works have revealed that sintered silicon nitride is susceptible to corrosion by acids, bases, saline solutions and hydrothermal treatments.[3–12] Only a few studies report corrosive attacks of the silicon nitride grains.[3–5,13] The common feature is the attack of the GBP[1,3,4,6,11,12,14,15] with an extent depending on various parameters such as pH, temperature, composition and concentration of acids or bases in the corrosive medium. Often, the corrosion process can be described by one or more of the following reactions[16]:

1. Acid–base-reactions:

$$Me_xO_y + 2yH^+ \rightarrow xMe^{(2y/x)+} + ½yH_2O$$

2. Hydration of metal oxides:

$$Me_xO_y + nH_2O \rightarrow Me_xO_y{\cdot}nH_2O$$

3. Hydrolysis of covalent bonds:

$$Si_3N_4 + 3(n+4)H_2O \rightarrow 3H_4SiO_4{\cdot}nH_2O + 4NH_3$$

* Corresponding author at: Eberhard Karls Universität Tübingen, Institute for Geoscience, Applied Mineralogy, Wilhelmstrasse 56, D-72074 Tübingen, Germany. Tel.: +49 7071 29 73 439; fax: +49 7071 29 30 60.
E-mail address: detlef.dierksen@uni-tuebingen.de (D. Dierksen).

0955-2219/$ – see front matter © 2010 Elsevier Ltd. All rights reserved.
doi:10.1016/j.jeurceramsoc.2010.12.001

The case of H_2SO_4 corrosion of silicon nitride ceramics is best investigated.[1,3,4,9–12,15–18] Exposures sometimes exceeding 400 h in up to 120 °C hot sulphuric acid were reported.[8,10–12,15,16] Together all cited works cover a wide range of experimental conditions with different sulphuric acid concentrations, exposure times and temperatures (Table 2). Most studies have shown a dissolution effect of the GBP within the "glass pockets" of triple points inside the silicon nitride grain network.

The GBP is often amorphous and therefore studies on glass corrosion can help to understand silicon nitride ceramics corrosion.[1,19–22] Previous works dealt with microbially influenced or direct microbial corrosion of glass.[23–28] The authors described several mechanisms for the microbial corrosion of glasses. Some organisms are able to use the compounds present in the glass either as growth substrate or as nutrient source.[23,28] Most of the described organisms belong to the fungi group and release different organic acids during their metabolic activity.

There is a lack of knowledge about microbial corrosion of such ceramics, even though the studies on abiotic corrosion of Si_3N_4-ceramics suggest that at least the sulphuric acid producing group of microorganisms should be able to corrode silicon nitride ceramics.

In this study we performed corrosion experiments with silicon nitride ceramics, which were immersed into bacterial cultures of the sulphuric-acid-producing strain *Acidothiobacillus ferrooxidans*. We compare the results to the corrosion in abiotic sulphuric acid systems with regard to corrosion rates, efficiency, grain boundary composition and structure.

2. Materials and methods

Corrosion experiments were carried out with commercially available Si_3N_4 (Kyocera SN220 M) on bending bars with dimensions of 4 mm × 3 mm × 45 mm. Some of the bars were cut to a different geometry with dimensions of 4 mm × 3 mm × 10 mm.

The corrosion experiments were conducted in 50 or 100 ml of either 5 mM H_2SO_4 (pH 2.0, "abiotic corrosion"), bacterial culture with *A. ferrooxidans* (acidophilic, pH ~2.0–2.5, "microbial corrosion") or culture medium without microorganisms in DSMZ-medium M71 as described by Tuovinen and Kelly[29] at a pH of 4.5. M71 was used as a non-corrosive standard. All experiments were performed at 30 °C in Erlenmeyer flasks with a fixed volume of corrosion media. These were closed with cellulose stoppers and fixed on a rotary shaker (150 rpm). The bacterial cultures grew until the required pH-range of 2.0–2.5 was reached, which lasted up to 5 days. The ceramic samples were then immersed into the cultures. Short bars (10 mm) were placed into 50 ml and long bars (45 mm) into 100 ml of culture medium. Abiotic control tests were performed by exposing bending bars to aqueous solutions of 5 mM H_2SO_4. The exposure time varied between 168.5 and 264 h.

One set of experiments was conducted to separate the influence of living bacteria in an acid environment from an acid environment set by bacteria. This was done because biochemical and biophysical interactions between the bacterial cells and the inorganic substratum might contribute to the corrosion process. On the other hand the bacteria do change chemistry of the acids during their life and this variation may be the reason for differences in the corrosion behavior. Thus exposure tests with two Si_3N_4-samples (SN220-20, -21; Table 1) in 50 ml of an appropriate culture supernatant were performed. The bacterial cultures were grown for 5 days before the cells were removed by centrifugation at 7500 × *g* and subsequent filtration with 0.22 μm cellulose acetate filters. These steps ensured the complete removal of bacteria, organic agglomerates and inorganic precipitates such as elemental sulphur from the medium. But the conditions of these experiments were similar to abiotic (pH = 2.0, T = 30 °C) and microbial treatments (pH 2.0–2.5, T = 30 °C). These experiments were conducted for a period of 240 h.

Before and after the corrosion experiments the ceramic samples were washed with acetone in an ultrasonic bath for 10 min, then rinsed with deionized water for 2 min and air-dried in a cabinet dryer for at least 2 h at 150 °C. After a cooling period of 2 h in an exsiccator the samples were weighed with a microbalance (d = ±0.01 mg, triplicate measurements).[11] During the abiotic exposure to sulphuric acid some of the ceramic bars were gravimetrically measured. This was not possible with microbially exposed samples because such a treatment would induce a loss of sterility. To confirm the gravimetric results of abiotically corroded samples, 2 bars were immersed into H_2SO_4 without intermittent weighing steps.

To determine and quantify the dissolution of yttrium and aluminium from the ceramic surface eluate (2 ml each) was sampled 6–7 times during each experiment. In case of bacterial cultures the samples were taken under sterile conditions to avoid microbial contamination. Each microbial eluate sample was centrifuged for 5 min at 20,000 × *g* and subsequently filtered through 0.22 μm syringe filters. This was done in order to remove residual bacterial cells, organic agglomerates and precipitates from the supernatant. The eluates were stored in tightly closed Eppendorf vials either at 4 °C (abiotic samples) or at −18 °C (microbial samples). The concentrations of dissolved yttrium and aluminium in the eluates were measured by ICP-MS (Perkin Elmer Elan 6000) and ICP-OES (Perkin Elmer Optima 5200), respectively. All eluate results were related to the geometrical surface area to obtain a measure of mass loss per surface area unit (μg/cm^2).

Cross sections of the Si_3N_4-bars for scanning electron microscopy (SEM) and electron microprobe (EMP) analysis were fixed in epoxy resin, polished and plasma etched with a CF_4–O_2-gas-mixture with a mixing ratio of 2:1. For qualitative EMP-linescans the samples were sputtered with carbon (max. thickness ~30 nm) and measured in 1, 2 and 5 μm steps to determine the corrosion penetration depth.

The microstructure of the samples, particularly the development of porosity, was analyzed by SEM, and taken as a sign for corrosion penetration. The preparation of the samples corresponded to that for EMP analysis, however in this case the samples were sputtered with platinum (thickness ~5 nm).

Table 1
Overview of samples.

Sample ID		Length [mm]	Exposure duration [h]	Medium	Eluate chemistry analyses	
					ICP-MS	ICP-OES
SN220-(BIO)	1	9.9	192.0	*Acidithiobacillus ferrooxidans* bacterial culture	Y	
	2	9.8	192.0			Al
	3	45.0	241.0		Y	
	4	45.0	241.0		Y	
	10	9.8	237.5		Y	
	11	9.9	237.5		Y	
	12	9.8	237.5		Y	
	13	45.0	236.5		Y	Al
	14	10.7	168.5		Y	Al
	15	9.9	236.5		Y	Al
	16	9.6	236.5		Y	
	17	9.9	236.5			Al
	20	10.0	239.5	*A. ferrooxidans* culture supernatant	Y	
	21	10.3	239.5		Y	
SN220-(ABIO)	7	9.7	249.5	5 mM H_2SO_4	Y	
	8	9.8	249.5		Y	
	9	10.0	249.5		Y	
	18	10.0	264.0		Y	Al
	19	10.6	264.0		Y	Al

3. Results

3.1. Gravimetry

The gravimetric measurements of the silicon nitride samples before and after exposure to microbial and abiotic corrosive media and M71 culture medium are shown in Fig. 1. Significant mass losses were observed from experiments performed in 5 mM H_2SO_4, with *A. ferrooxidans* and the culture supernatant, whereas exposure to the sterile M71 medium did not result in any mass loss.

The (abiotic) mass loss in 5 mM H_2SO_4 is clearly not a linear function of the exposure time, even though two samples without intermediate weighing steps gave somewhat higher losses at long times (dashed arrow in Fig. 1). The problem of kinetics is addressed below in a later section of this paper.

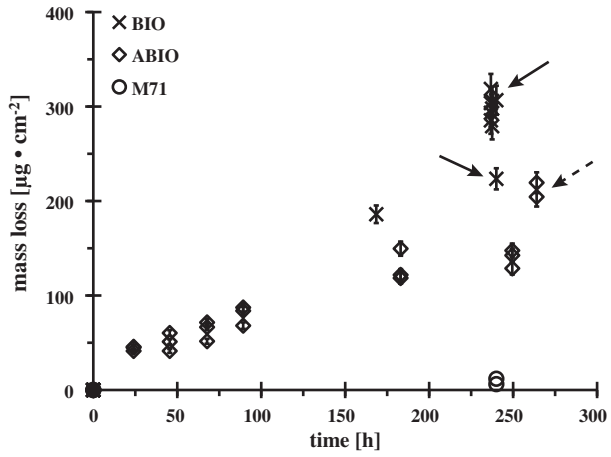

Fig. 1. Normalized mass loss after exposure in *Acidithiobacillus ferrooxidans* bacteria culture (BIO), 5 mM H_2SO_4 (ABIO) and unmodified culture medium medium (M71). Full arrows show mass loss values of samples exposed into culture supernatant after growth and removal of bacteria. The dashed arrow points at the mass loss values of abiotically corroded samples without intermittant weighing steps.

Samples from solutions with living bacteria were kept in the solution without interruption. It is therefore impossible to deduce a kinetic law from the data. However, the mass loss is fairly well defined and significantly higher than loss in abiotic treatments of equal duration. An overview of previously published mass loss values from other authors and their comparison to our data is given in Table 2.

One of the samples, which were exposed to the bacterial supernatant (i.e. the solution of biological history without living bacteria) had in one case a mass loss in agreement with those from exposure to *A. ferrooxidans* culture. However, the second sample gave a lower value (307–224 µg/cm^2, Fig. 1, full arrows). The question, whether living bacteria do influence the process, can therefore not be answered from our gravimetric data.

3.2. Eluate chemistry

The results of eluate analyses allow the determination of normalized mass losses over time for individual elements. These data enable us to calculate models to describe corrosion kinetics.

The concentrations of dissolved yttrium and aluminium in the eluates were recalculated to mass loss of yttria and alumina per surface area to compare the results of gravimetry and eluate chemistry (Fig. 2). From Fig. 2a it can be seen that microbial corrosion led to higher dissolution rates of yttria, although we performed our abiotic experiments under similar conditions. No yttria loss was observed when the ceramics were exposed to the original culture medium M71.

The spread in the values for microbial yttria dissolution is much higher than those from abiotic corrosion in H_2SO_4. Nonetheless it is obvious that leaching of yttria by *A. ferrooxi-*

Table 2
Mass loss values for yttria bearing Silicon nitride ceramics in sulphuric acid—previously published data compared to this work.

Author	H_2SO_4-concentration [mol/l]	pH	T [°C]	Exposure time, max. [h]	Mass loss** ($-\Delta m$) [mg/cm^2]
Okada et al.[8]	1.5–6.0 (3.0–12.0 N*)	<0	104–120	72	~0.3–3.2
Monteverde et al.****,[12]	1.8–3.6	<0	25–70	400	~1.6–2.9
Herrmann et al.[4]	0.5 (1.0 N*)	0	90	200	20.02
Schilm et al.[10]	0.5 (1.0 N*)	0	60–101	240	~9.0–20.0
Schilm et al.[15]	0.00005–3.0	<0–4	90	300	~0–26.0
This work					
SN220 (BIO)	0.0016–0.005	2.0–2.5	30	241	0.19–0.32***
SN220 (ABIO)	0.005	2.0	30	264	0.13–0.22***

* Data as published.
** Approximate values were taken out of published diagrams.
*** Values were rounded off to two decimal places.
**** Different additive composition of samples.

dans is significantly enhanced in comparison to the corrosion in H_2SO_4 under similar pH conditions. The data of Fig. 2a include the values for the exposure to the culture supernatant, which cannot be distinguished from microbial corrosion in presence of *A. ferrooxidans*.

In contrast, the dissolution of alumina does not show differences between microbial and abiotic corrosion (Fig. 2B). The superficial dissolution kinetics of alumina appears to be linear with exposure time, independent from the corrosion method.

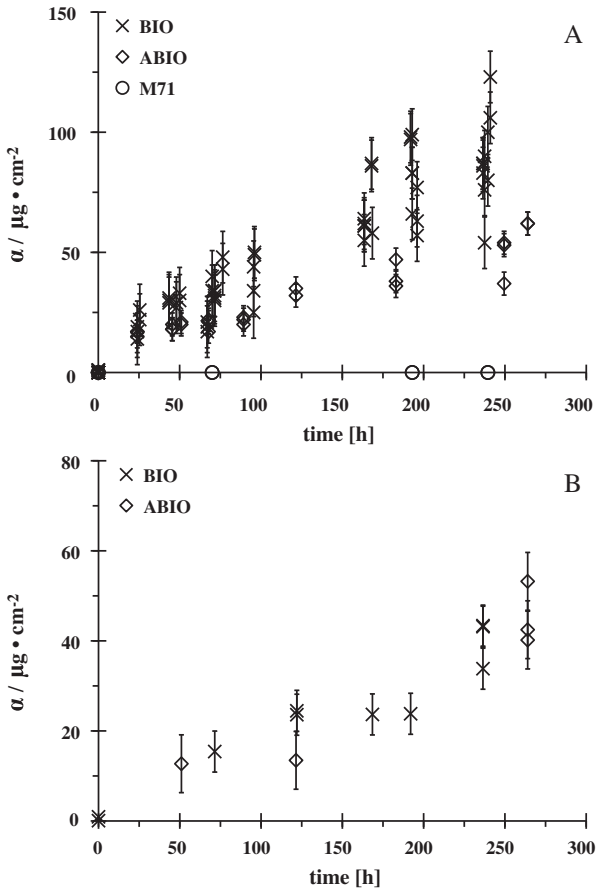

Fig. 2. A, B: Normalized mass loss α, data based on eluate chemistry. (A) Yttria mass loss with clear differences between microbial (BIO) and abiotic (ABIO) corrosion; unmodified culture medium used as standard (M71). (B) Alumina mass loss without differences between microbial and abiotic corrosion.

3.3. Electron microprobe (EMP) linescans

EMP-linescans were performed perpendicular to the sample surface on cross sections. Their results showed the element distribution from the ceramic surface to the unmodified interior. These analyses provided therefore information about the penetration depths of the corrosion experiments. The gravimertric and eluate chemistry results were confirmed by these linescans. The linescans were conducted on samples, which were exposed for 237.5 (BIO) and 249.5 (ABIO) hours to the corrosive media and are shown in Fig. 3. They allow an estimation of the penetration depths directly from the data of the counts of the elements yttrium, aluminium and the associated oxygen. The linescans exhibited three zones, which may be attributed to: the embedding agent (I), the corrosion (II) and the bulk zone (III). The penetration depths depend on the corrosion medium (BIO, ABIO).

A shift of Y-, Al- and O-concentrations from (II) to (III) was observed in both BIO and ABIO linescans. Within the corrosion zone the samples showed lower concentrations than in the bulk zone. Regarding the microbially treated (BIO) samples the element concentrations from corrosion to bulk zone increased with clear borders between the zones. The microbial corrosion resulted in an almost complete depletion of Y whereas Al and O were depleted partially. Si- and N-linescans did not show any corrosion influence.

Similar results were gathered during abiotic corrosion in sulphuric acid (ABIO).

A detailed analysis of the results in Fig. 3, however, revealed interesting differences. In contrast to microbial leaching the abiotic corrosion process did not lead to a complete superficial dissolution of yttria. Instead we observed gradual changes with depths rather than clear steps in the element concentrations. In contrast to BIO-results the ABIO-scans showed also gradual increases of Si and N.

Since the EMP-linescans indicated different zones within the corroded samples, the widths of the corrosion zones depicted the depth of corrosion penetration. Due to a beam diameter of 2 µm and an excitation volume of several µm^3 the zones cannot be separated with an accuracy better then 4 µm. The microbial corrosion (BIO) affected a zone of 8–16 µm depth (transition zones marked by grey shadings) whereas

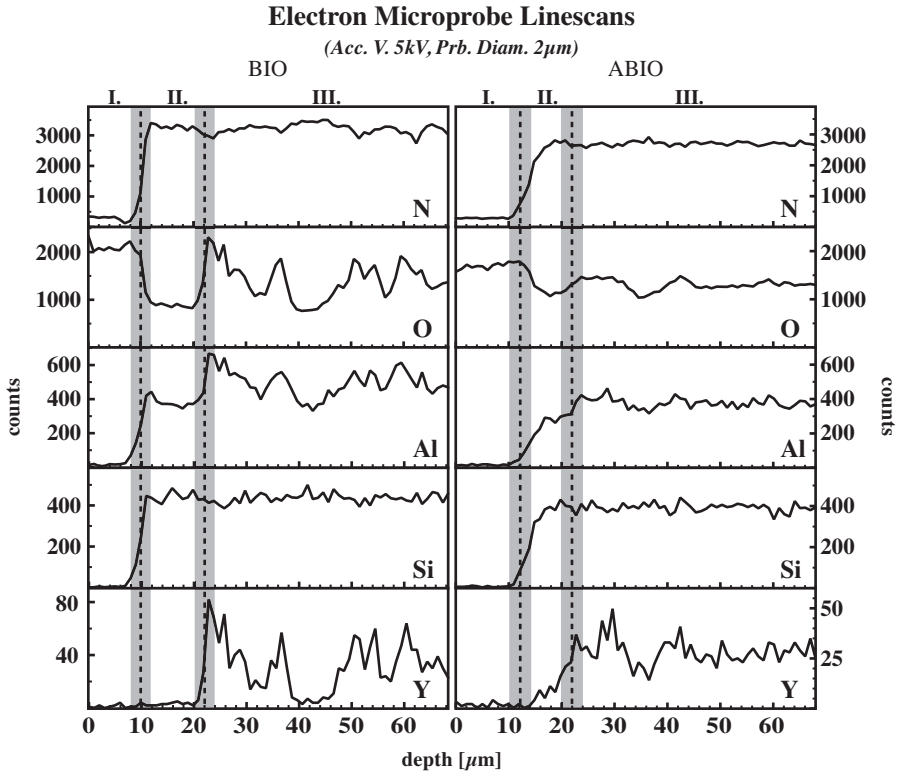

Fig. 3. EMP-linescans of microbially (BIO) and abiotically (ABIO) corroded Si_3N_4-samples show three clearly distinguishable zones: (I) epoxy as embedding agent, (II) corrosion and (III) bulk zone. The dashed lines mark the transitions between the three zones within uncertainty ranges (grey shadings). Deeper penetration occurred after microbial corrosion (8–16 μm including the transition zones) compared with abiotic corrosion (6–14 μm). Corrosion affected O-, Al- and Y-concentrations while N- and Si-concentrations were not influenced.

the abiotic corrosion (ABIO) reached a penetration depth of approximately 6–14 μm.

3.4. Microstructure by scanning electron microscopy (SEM)

The microstructures of the corroded samples as investigated by a scanning electron microscope (SEM) are shown in Fig. 4. Both corrosion methods caused surface embrittlement, evidenced by numerous preparation marks at the sample surfaces like pits from cutting and polishing (Fig. 4A–C), absent in untreated samples. The corrosion did not intrude homogeneously but resulted in an undulated corrosion front. Fig. 4B and C shows that the corrosive medium penetrated preferentially along tight channels and vein-like pathways.

Fig. 4D–H reveals different states of dissolution of the amorphous glass phase (GBP) appearing within the triple points between the Si_3N_4-grains, depending on the experimental method. Microbial corrosion resulted in an almost complete dissolution of the GBP without any visible residuals (Fig. 4E and G). Inside the corrosion zone most of the Si_3N_4-grains appear "clean" and show their typical hexagonal shape. Even small cavities within the structure lack a bonding glassy phase (Fig. 4G).

Abiotic sulphuric acid corrosion caused a similar dissolution of the GBP only within the upper surface area (up to 3–4 μm depth, Fig. 4D and F) and a partially dissolved amorphous phase inside the deeper corrosion zone (Fig. 4H). This graded dissolution with distinct glassy residuals caused an irregular coverage of Si_3N_4-grains. Single grains and grain boundaries cannot be separated in detail (Fig. 4H).

4. Discussion

A higher efficiency of microbial corrosion compared to abiotic corrosion under similar conditions was indicated in this study through various analytical techniques. Eluate chemistry results regarding the superficial dissolution of yttria correlate well with gravimetric measurements and SEM- and EMP-analyses. An almost complete dissolution of the amorphous glassy phase inside the corrosion zone of the microbially treated Si_3N_4-samples suggests that the yttria-concentration decreased towards zero within that domain. It is known that yttria is normally enriched inside the "glassy pockets" whereas alumina can be found in the "glassy pockets", the stable glassy films between individual grains[1] and inside the grains by SiAlON formation. So all the yttria is available for the corrosive attack but alumina only partially.

Our results concerning yttria-dissolution-mediated mass loss distinguish microbial (BIO) and abiotic (ABIO) corrosion. Therefore the results of Y-eluate-chemistry were used to calculate both the mass loss per surface area (Fig. 2) and to evaluate the possible corrosion kinetics based on standard models[5,10,30,31] for planar sample geometry with unidimen-

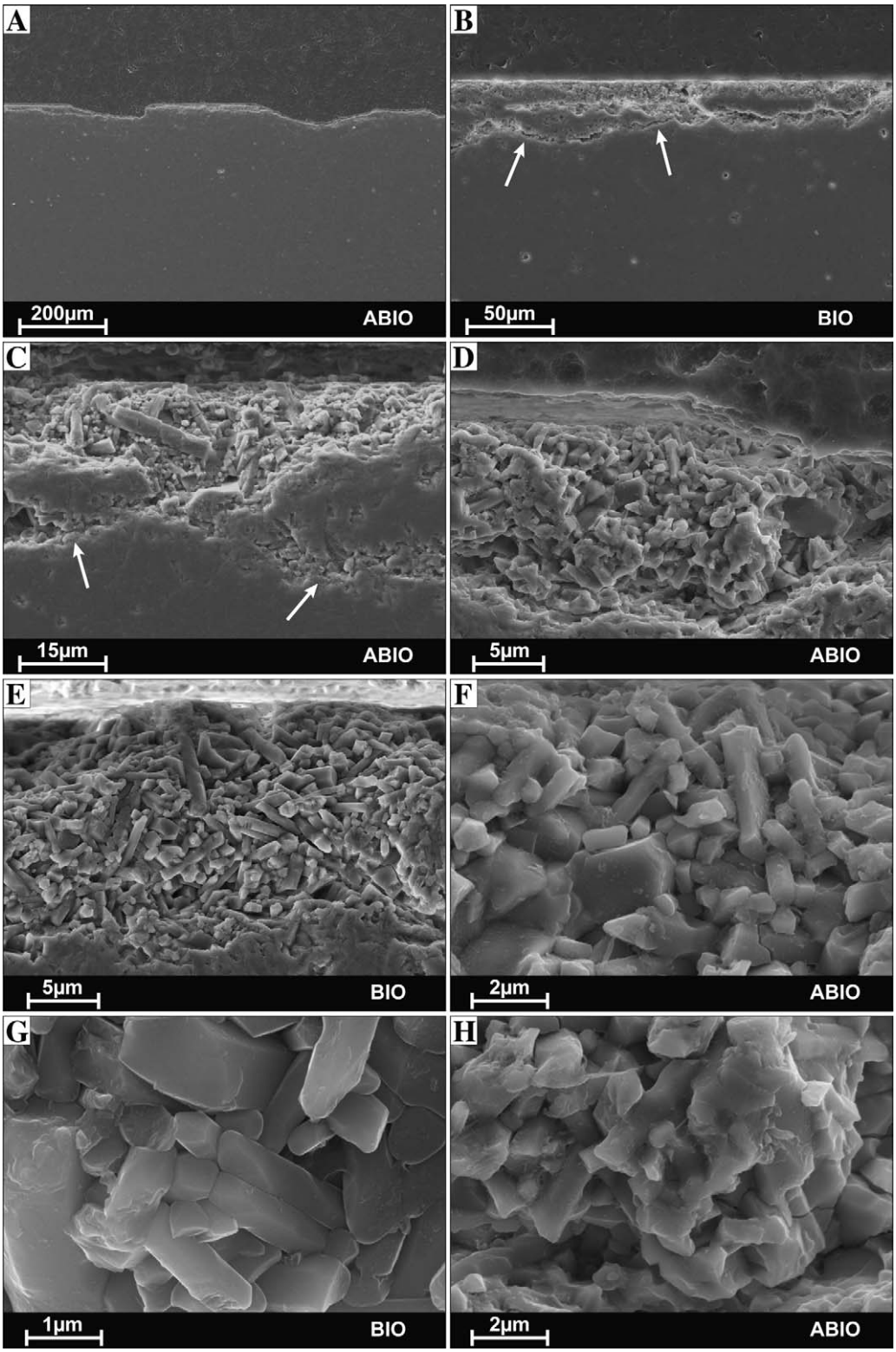

Fig. 4. (A–H) SEM micrographs of corroded silicon nitride samples; (A) pits and excavations caused by preparation of samples; (B, C) heterogeneous corrosion front, corrosive penetration through vein-like channels (arrows); (E, G) microstructure of corrosion zone after microbial corrosion: complete dissolution of grain boundary phase in triple points, pockets and small cavities (G); (D, F and H) microstructure of corrosion zone after abiotic corrosion: graded dissolution of grain boundary phase (F: upper corrosion zone, grain boundary phase almost completely dissolved; H: deeper corrosion zone with residues).

sional mass transport.[5] Linear kinetics could be caused by a reaction-controlled corrosion whereas parabolic kinetics are usually due to diffusion-control. A mixed reaction-control may be assumed for more complex corrosion patterns and in the simplest case includes the assumption that the basic laws operate simultaneously.

We have no reason to expect sudden processes in the initial or heating-up period. Therefore we may investigate our data forcing any model to start with 0 mass loss at time 0. Then the basic laws for the variable α, which is here the measure of corrosion progress in terms of the mass loss per unit area, become:

1. Linear (reaction-controlled):

$$\alpha(t) = k_l \cdot t \tag{1}$$

The linear rate constant k_l in SI-units is then $\mathrm{kg\,m^{-2}\,s^{-1}}$.

2. Parabolic (diffusion-controlled):

$$\alpha(t) = \sqrt{k_p \cdot t} \tag{2}$$

The parabolic rate constant for mass loss k_p has the unit $\mathrm{kg^2\,m^{-4}\,s^{-1}}$.

3. Mixed reaction-control:

$$\alpha(t) = k'_p \cdot \sqrt{t} + k_l \cdot t \tag{3}$$

The correlations between experimental data and calculated models are given in Fig. 5A–C, the extracted rate constants and their standard deviations are given in Table 3. From Fig. 5A it is obvious that a linear fit would either violate the condition that mass loss is zero at time zero or include systematic misfit at short run times for both microbial (BIO) and abiotic (ABIO) corrosion.

A parabolic fit (Fig. 5B) is acceptable for the abiotic corrosion (ABIO) but clearly overestimates the BIO-data at times below 100 h. A diffusion-controlled kinetic law is conceivable for the ABIO-data, because we have considerable amounts of amorphous grain boundary phase remaining and the corrosion zone has a chemical gradation in yttria.

Nonetheless both data sets are fitted best by the mixed law (Eq. (3), Fig. 5C). Looking at the fitted values for the mixed model (Table 3), it is plain that the linear constant k_l is much smaller for the ABIO-data then for those from biotic experiments, while the k_p values are equal within their uncertainty. This is compatible with the data presented above, because the latter data set showed an almost complete loss of grain boundary

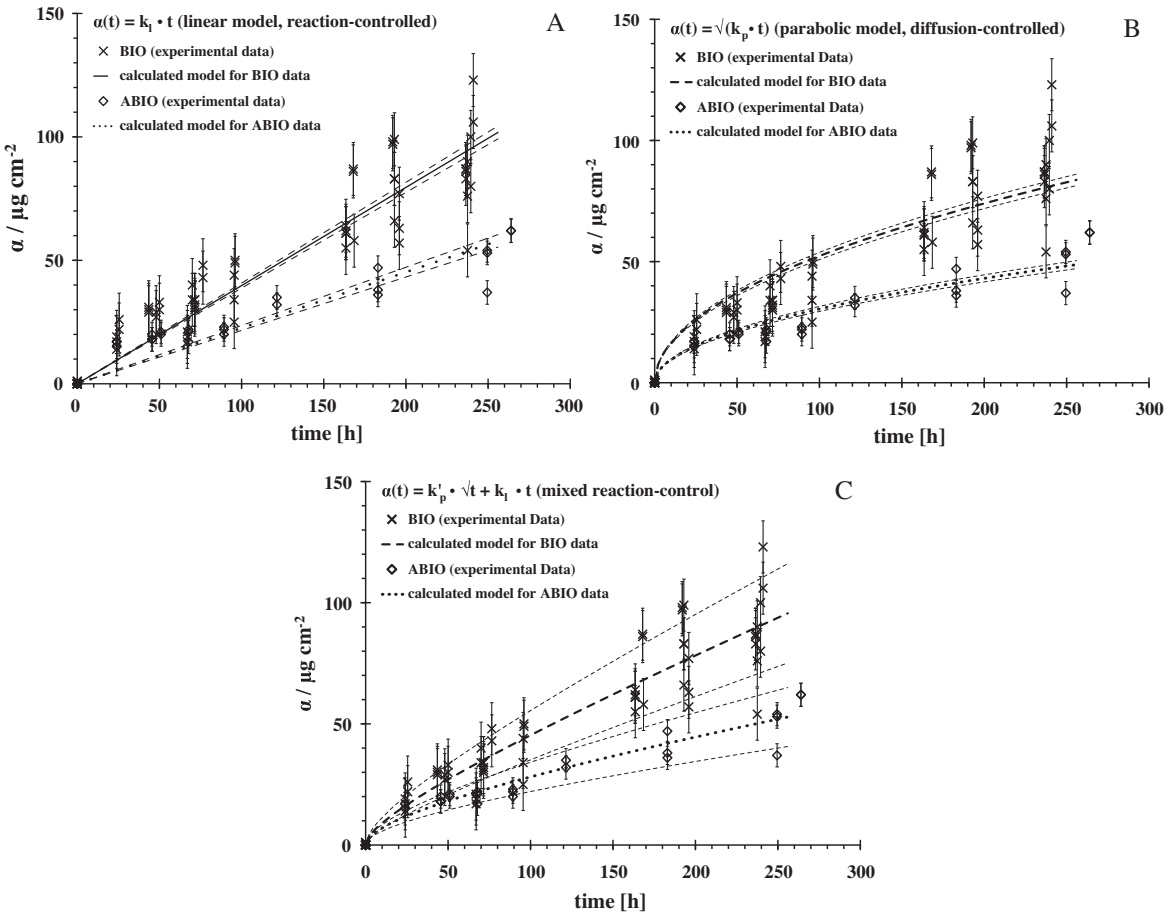

Fig. 5. (A–C) Normalized mass loss and calculated corrosion kinetic models for yttria-dissolution (values with standard deviations in Table 3). (A) Linear model for reaction-controlled corrosion.[1,2] (B) Parabolic model for diffusion-controlled corrosion.[1,2] (C) Mixed reaction-control with reaction- and diffusion-controlled fractions.[1–3]

Table 3
Rate constants.

		$k_l \times 10^{-5}$ [kg m^{-2} s^{-1}]	$k_p \times 10^{-10}$ [kg^2 m^{-4} s^{-1}]	R^2
Linear	BIO	0.3977 ± 0.0102		0.9560
	ABIO	0.2261 ± 0.0099		0.9495
Parabolic	BIO		27.3832 ± 0.0219	0.9470
	ABIO		9.2799 ± 0.0106	0.9691
Mixed reaction control	BIO	2.1224 ± 0.5787	0.0508 ± 0.0019	0.9632
	ABIO	1.9955 ± 0.3456	0.0067 ± 0.0007	0.9774

phase from the triple points. The recession of this phase must induce a relatively large linear term in (Eq. (3)). Likewise the small linear term in the fit of the ABIO-data is compatible with a small zone of total loss of the phase from the assemblage near the surface.

The EMP-linescans of Fig. 3 show that the higher normalized mass loss values for microbial corrosion are not only a result of the complete dissolution of the glassy phase in BIO samples but also of a deeper penetration of the microbially modified, corrosive medium. The ABIO-linescan shows a total dissolution of Y only within the upper part of the corrosion zone (max. 4 μm) and a gradation in the lower zone, indicating that the remaining amorphous phase is not a corrosion-induced secondary precipitate but part of the original amorphous grain boundary phase. A leaching process is therefore assumed to dominate the scale formation.

The loss of alumina in the BIO-samples (Fig. 2B) is linear, which fits to the yttria loss kinetics of the same data set. However, the rather parabolic kinetics of yttria-loss from ABIO samples is not mirrored by the BIO data set despite the gradation in alumina in zone II seen in Fig. 3. This is difficult to explain, even though we know that part of the alumina is not incorporated within the triple points but either within the glassy films between individual grains or in the SiAlON-phase at the Si_3N_4-grain surfaces. Currently we have no good explanation for this discrepancy, which is, however, based on a small number of data.

The reasons for the higher efficiency of microbially induced corrosion are still unknown. Our experiments with microbially modified culture medium (bacterial supernatant) indicate no direct influence of the microorganisms by biochemical and biophysical interactions between the cells and the ceramic substrate surface. This suggests that the composition of the culture supernatant caused the more efficient corrosion. With regard to the initial composition of the culture medium M71 (KH_2PO_4 3.00 g, $MgSO_4{\cdot}7H_2O$ 0.50 g, $(NH_4)_2SO_4$ 3.00 g, $CaCl_2{\cdot}2H_2O$ 0.25 g, $Na_2S_2O_3{\cdot}5H_2O$ 5.00 g, deionized H_2O 1000 ml) it may be possible to conclude that microbial activity within the growth phase led to an enrichment of sulfate and chloride. Magnesium, calcium, sodium and ammonium are used for the metabolic activity. Thiosulfate is oxidized to sulphuric acid[29] whereas phosphate is used as a buffer and is therefore not supposed to promote the corrosive process. The higher biological corrosion efficiency is probably due to organic compounds formed and released to the supernatant as a result of the metabolic activity. These organic compounds could include organic acids, alcohols, carbohydrates or other carboxylic-group containing chemical compounds—all compounds are known to be able to complex metal ions. Theoretically it is possible that at each step of the TCA-[32,33] and Calvin-Cycle[34] organic compounds are released by the cells into the surrounding environment. The works of Valdès et al.[35] and Hold et al.[36] support the theory that these organisms do release additional organic compounds which could promote the corrosive effect of sulphuric acid. Further experiments are being conducted to identify these additional compounds that may enhance the corrosive process.

5. Conclusions

In this study a higher efficiency of corrosion by bacterial cultures with *Acidithiobacillus ferrooxidans* was shown compared to abiotic corrosion under similar conditions of pH, temperature and exposure time. The differences concern normalized mass loss, corrosion kinetics and penetration depths. A removal of the organisms by centrifugation and filtration gave a bacterial supernatant, which had equal or similar corrosion power. Therefore biophysical and biochemical interactions at the cell–substratum-interface are probably not responsible for the differences. Until now, the reasons for the higher microbial corrosion rates are not fully understood, but we believe that this is due to the bacterial release of additional corrosion-supporting compounds like organic acids and complexing agents. However, so far our anlytical approaches to identify such substances were not successful.

Acknowledgements

Deutsche Forschungsgemeinschaft, SPP HAUT 1299, for funding this project Dr. Joern Breuer, Landesanstalt für Landwirtschaftliche Chemie, University of Stuttgart-Hohenheim, Germany, for ICP-MS measurements Dipl. Ing. Marco Riva and Dr. Rainer Oberacker, Institut für Keramik im Maschinenbau, University of Karlsruhe, Germany, for providing insights into ceramic processing PD Dr. Thomas Wenzel, Institut für Geowissenschaften, University of Tübingen, Germany, for help and discussion relating to electron microprobe analyses Indra Gill-Kopp, Institut für Geowissenschaften, University of Tübingen, Germany, for excellent preparation of ceramic samples.

References

1. Petzow G, Herrmann M. Silicon nitride ceramics. In: *High performance non-oxide ceramics II*. 2002. p. 47–167.
2. Subramaniam A, Koch CT, Cannon RM, Rühle M. Intergranular glassy films: an overview. *Mater Sci Eng A* 2006;**422**:3–18.

3. Herrmann M, Schilm J, Hermel W, Michaelis A. Corrosion behaviour of silicon nitride ceramics in aqueous solutions. *J Ceram Soc Jpn* 2006;**114**(11):1069–75.
4. Herrmann M, Schilm J, Michael G, Meinhardt J, Flegler R. Corrosion of silicon nitride materials in acidic and basic solutions and under hydrothermal conditions. *J Eur Ceram Soc* 2003;**23**:585–94.
5. Nickel KG, Gogotsi YG. Corrosion of hard materials. In: Riedel R, editor. *Handbook of ceramic hard materials*. Weinheim: VCH-Wiley; 2000. p. 140–82.
6. Nickel KG, Seipel B. Corrosion penetration monitoring of advanced ceramics in hot aqueous fluids. *Mater Res* 2004;**7**(1):125–33.
7. Okada A, Iio S, Asano T, Kokaji A, Takahashi H, Yoshimura M. Corrosion behavior of silicon nitride ceramics in aqueous solutions (Part 1): effects of testing condition and various corrosive solutions. *J Ceram Soc Jpn* 1991;**99**(1156):1260–4.
8. Okada A, Iio S, Asano T, Yoshimura M. Corrosion behavior of silicon nitride ceramics in aqueous solutions (Part 2): weight loss and bending strength tested in boiling sulfuric acid. *J Ceram Soc Jpn* 1992;**100**(1157):80–3.
9. Okada A, Yoshimura M. Mechanical degradation of silicon nitride ceramics in corrosive solutions of boiling sulphuric acid. *Key Eng Mater* 1996;**113**:227–36 [Corrosion of advanced ceramics].
10. Schilm J, Herrmann M, Michael G. Kinetic study of the corrosion of silicon nitride materials in acids. *J Eur Ceram Soc* 2003;**23**:577–84.
11. Seipel B, Nickel KG. Corrosion of silicon nitride in aqueous acidic solutions: penetration monitoring. *J Eur Ceram Soc* 2003;**23**(4): 595–602.
12. Monteverde F, Mingazzini C, Giorgi M, Bellosi A. Corrosion of silicon nitride in sulphuric acid aqueous solution. *Corros Sci* 2001;**43**: 1851–63.
13. Seipel B. *Korrosion von Silziumnitrid und zirkonoxidverstärktem Aluminiumoxid in wässrigen Lösungen unter Durchflußbedingungen, in Institut für Geowissenschaften*. Tübingen: Eberhard-Karls-Univertität Tübing; 2003. p. 182.
14. Bellosi A, Graziani T, Monteverde F. Degradation behaviour of silicon nitride in aqueous acid solutions. *Key Eng Mater* 1996;**113**:215–26 [Corrosion of advanced ceramics].
15. Schilm J, Herrmann M, Michael G. Corrosion of Si_3N_4-ceramics in aqueous solutions: Part 2. Corrosion mechanisms in acids as a function of concentration, temperature and composition. *J Eur Ceram Soc* 2007;**27**(12):3573–88.
16. Schilm J. *Korrosion von gasdruckgesinterten Si3N4-Keramiken in Säuren, in Fak. f. Maschinenbau*. Freiberg: Universität Freiberg; 2004. p. 159.
17. Iio S, Okada A, Asano T, Yoshimura M. Corrosion behavior of silicon nitride ceramics in aqueous solutions (Part 3): corrosion behavior in hot sulfuric acid and microstructure of corroded layer. *J Ceram Soc Jpn* 1992;**100**(1163):965–7.
18. Seipel B, Nickel KG. Protection of silicon nitride ceramics against corrosion in acidic aqueous solutions by enforced internal passivation. *Ceram Int* 2004;**30**(2):267–71.
19. Becher PF, Sun EY, Hsueh C-H, Alexander KB, Hwang S-L, Waters SB, et al. Debonding of interfaces between beta-silicon nitride whiskers and Si–Al–Y oxynitride glasses. *Acta Mater* 1996;**44**(10):3881–93.
20. Cinibulk MK, Thomas G, Johnson SM. Oxidation behavior of rare-earth disilicate-silicon nitride ceramics. *J Am Ceram Soc* 1992;**75**(8):2044–9.
21. Lange H, Wötting G, Winter G. Siliciumnitrid—vom Pulver zum keramischen Werkstoff. *Angew Chem* 1991;**103**(12):1606–25.
22. Ziegler G, Heinrich J, Wötting G. Review: relationships between processing, microstructure and properties of dense and reaction-bonded silicon nitride. *J Mater Sci* 1987;**22**(9):3041–86.
23. Drewello R, Nüssler M, Weissmann R. Mikrobielle Werkstoffzerstörung—Simulation, Schadensfälle und Gegenmaflnahmen für anorganische nichtmetallische Werkstoffe: Korrosion von Modellgläsern durch mikrobielle Stoffwechselprodukte. *Mater Corros* 1994;**45**(2):122–4.
24. Drewello R, Weissmann R. Attack on Glass. In: Heitz E, Flemming H-C, Sand W, editors. *Microbially influenced corrosion of materials: scientific and engineering aspects*. Telos: Springer-Verlag; 1996. p. 339–52.
25. Drewello R, Weissmann R. Microbially influenced corrosion of glass. *Appl Microbiol Biotechnol* 1997;**47**(4):337–46.
26. Grambow B. Corrosion of glass. In: Revie R, editor. *Uhlig's corrosion handbook*. New York: John Wiley & Sons; 2000. p. 411–37.
27. Kaiser J-P, Trümpler S, Raschle P. Wachstum von Taeniolina deightonii auf mittelalterlichen Gläsern. *Werkstoffe und Korrosion* 1994;**45**:125–7.
28. Staudigel H, Chastain RA, Yayanos A, Bourcier W. Biologically mediated dissolution of glass. *Chem Geol* 1995;**126**(2):147–54.
29. Tuovinen OH, Kelly DP. Studies on the growth of *Thiobacillus ferrooxidans*. *Arch Microbiol* 1974;**98**(1):351–64.
30. Nickel KG. Zur Modellierung der Kinetik von Korrosionsprozessen. *Ceram Forum Int Beihefte* 1999;**14**(1):7–17.
31. Conradt R, Roggendorf H, Scholze H. A contribution to the modelling of the corrosion mechanisms of HLW glasses. *Mater Res Soc Symp Proc* 1985;**44**:155–62.
32. Kornberg H. Krebs and his trinity of cycles. *Nat Rev Mol Cell Biol* 2000;**1**(3):225–8.
33. Krebs HA. The history of the tricarboxylic acid cycle. *Perspect Biol Med* 1970;**14**(1):154–70.
34. Wilson AT, Calvin M. The photosynthetic cycle. CO_2 dependent transients. *J Am Chem Soc* 1955;**77**(22):5948–57.
35. Valdes J, Pedroso I, Quatrini R, Dodson R, Tettelin H, Blake R, et al. *Acidithiobacillus ferrooxidans* metabolism: from genome sequence to industrial applications. *BMC Genomics* 2008;**9**(1):597.
36. Hold C, Andrews BA, Asenjo JA. A stoichiometric model of *Acidithiobacillus ferrooxidans* ATCC 23270 for metabolic flux analysis. *Biotechnol Bioeng* 2009;**102**(5):1448–59.